

Thermal dynamics-based mechanism for intense laser-induced material surface vaporization

N KUMAR*, S DASH, A K TYAGI and BALDEV RAJ
Materials Science Division, Indira Gandhi Centre for Atomic Research,
Kalpakkam 603 102, India
*Corresponding author. E-mail: nkumar@rambler.ru

MS received 27 November 2006; revised 27 February 2008; accepted 27 May 2008

Abstract. Laser material processing involving welding, ablation and cutting involves interaction of intense laser pulses of nanosecond duration with a condensed phase. Such interaction involving high brightness radiative flux causes multitude of non-linear events involving thermal phase transition at solid–liquid–gas interfaces. A theoretical perspective involving thermal dynamics of the vaporization process and consequent non-linear multiple thermal phase transitions under the action of laser plasma is the subject matter of the present work. The computational calculations were carried out where titanium (Ti) was treated as a condensed medium. The solution to the partial differential equations governing the thermal dynamics and the underlying phase transition event in the multi-phase system is based on non-stationary Eulerian variables. The Mach number M depicts significant fluctuations due to thermal instabilities associated with the laser beam flux and intensity. A conclusive amalgamation has been established which relates material surface temperature profile to laser intensity, laser flux and the pressure in the plasma cloud.

Keywords. Pulsed laser–material interaction; plasma cloud; phase transition.

PACS Nos 42.62.-b; 42.62.Cf; 44.10.+i

1. Introduction

Evaporation from a surface irradiated with intense laser beam is an important process affecting the energy transfer, melt hydrodynamics and chemical composition of a work piece during laser-induced evaporation event. A model to compute solid surface temperatures below the critical temperature was developed by Semak and Matsunawa [1]. In particular, their model provided the value of evaporation recoil pressure, a dominant factor which determines melt motion at elevated surface temperatures.

A semi-analytical method has been developed and applied to analyse spatial and temporal distributions of temperature on material surface. This was studied by Gospavic and Serkovic [2]. Finite diameter cylindrical configuration with finite and infinite lengths has been considered. For solving the governing partial

differential equations (PDEs), the Laplace transform and the Fourier method of variables separation were used. In this way, instead of the original governing PDEs, ordinary differential equations (ODEs) could be solved. Particular solutions of the ordinary differential equations were used for arriving at a general solution which was expressed in terms of a series of particular solutions pertaining to evaporation process. The unknown coefficients in the series of particular solutions were determined using the boundary and initial conditions. The laser–material interaction was represented using a thermal model. These interactions for a case of the high power laser impacts in pulsed and continuous regimes were analysed. The incident intensity of laser radiation was kept under a critical value. Using these methods, the temperature field distribution was obtained in the Laplace transform domain, as attempted by Gospavic and Serkovic [2].

Suitable thermal boundary conditions were deduced by means of a ray-tracing procedure and the finite volume method was used to solve the hydrodynamic equations governing the recoil vapour flow. A steady-state solution gives the distribution of the vapour phase parameters consisting of the density, pressure, temperature and Mach number. The influence of the ambient pressure on the vapour flow is also investigated. Occurrence of friction phenomena between the vapour and the material surface resulting in uniform distribution of the pressure was observed. It is noted that the stabilizing effect of friction at low ambient pressures assumes importance as discussed by Chichkov *et al* [3]. Formulation based on theoretical solution to the material surface vaporization caused by intense laser beam has fundamental and technological significance. This is because there are considerable difficulties for experimental investigation of these physical phenomena. Mathematical description of these processes need complicated system of non-linear partial differential equations which are analytical only under exceptional circumstances. Therefore, numerical solution of the vaporization phenomena has become a subject matter of investigation by Semak and Matsunawa [1] and Chichkov *et al* [3]. The theoretical model presented by Cho and Na [4] is compatible especially for surface ablation, because this model ignores the effect of metal vapour in the keyhole area.

But all these methods mentioned above are not sufficient to explain the time step grid coordinates which account for thermal dynamics-induced movement on the material surface caused by the impact of nanosecond laser pulse. There is no physical correlation between the amount of laser absorption with the rate of evaporation. The absence of generation of sound wave (Mach number) does not represent the full picture of the velocity of the intensive evaporation in time domain with boundary variables.

This paper describes the role of incident laser intensity and pulse duration on vaporization dynamics. It also tries to define the underlying physical phenomena associated with high-power laser beam–condensed matter interaction. When a moderately intense laser beam with parameters $I \leq 10^8 \text{ W/cm}^2$, $\lambda = 1.064 \mu\text{m}$ and 5 ns confront a condensed phase causing absorption of significant portion of radiation, the vaporization process for this pulse duration becomes negligibly small. Certain fraction of laser beam intensity is sufficient to ionize the material in Knudsen layer causing intense vaporization. A recoiling homogeneous plasma envelope develops near the material surface with certain reaction phase velocity. Numerical calculations on the above scenario are based on thermal dynamic response,

quantified in terms of Mach number variation in time and spatial domain. The process is completed in three stages. Initially it is sonic ($M = 1$) evaporation due to beam absorption. It is followed by condensation during the period of plasma formation and expansion. The re-initiation of evaporation in subsonic ($M < 1$) region follows this. A supersonic ($M > 1$) regime occurs after the partial brightening of the plasma that expands outward from the material surface. To achieve numerical solutions to this problem we have taken non-stationary equations from radiative gas dynamics. These equations describe thermal dynamics in the vapour flux transport in terms of Eulerian variables defined with finite volume time step functional boundaries. The boundary value heat conduction–convection problem is addressed in a moving coordinate system to obtain thermal dynamics of vaporization front propagating across the Knudsen layer. Such rigorous understanding of thermal dynamics of laser surface vaporization process also lays the basis to analyse technological processes like keyhole generation during laser welding, cutting and laser material ablation.

2. Thermal dynamics of surface vaporization and non-linear thermal phase transition

Laser ablation of solid targets by 0.2–5000 ps Ti:sapphire laser pulses are analysed. This lays the basis for obtaining qualitative explanations of experimental results. Such an approach helps in deriving precise material evaporation conditions through the application of femtosecond lasers as described by Shirk and Molian [5]. It is also seen that as pulse width increases and intensity decreases, laser damage becomes a stochastic process in which the ultrashort pulsed, high intensity light causes optical breakdown. This phenomenon is coupled with lack of significant thermal conduction, greatly improves the precision of ultrashort pulsed laser-based micromachining developed by Sy-Bor Wen *et al* [6] and Chen and Wang [7]. Laser ablation of copper with a 4 ns laser pulse at 1064 nm was studied with a series of synchronized shadowgraphs (100 fs laser pulses at 400 nm). The emission images (spectral line at 515 nm) were obtained. Data were obtained at two different laser pulse energies (10 and 30 mJ). The background gases (He, Ne and Ar) at atmospheric pressure were used by Chen and Wang [7] and Richards and Walsh [8]. The laser energy conversion ratio and the amount of sample vaporized for ablation in each condition were obtained by the theoretical analysis. These analyses reveal the presence of external shock wave, internal shock wave and contact surface between the titanium (Ti) vapour and the background gas. All these three quantities were measured from shadowgraph and emission images. The results showed that E , the amount of energy that is absorbed by the Ti vapour, decreases as the atomic mass of the background gas increases. The mass of the sample, m , converted into vapour, is almost independent of the background gas studied by Chen and Wang [7] and Richards and Walsh [8]. A physical interpretation is given based on the phenomena observed in shadowgraph. The emission images were acquired during the first tens of nanoseconds after the beginning of the laser pulse for ablation in different background gases. In addition, the internal shock wave was observed in the emission images during the first tens of nanoseconds after the laser pulse which strikes the surface of Ti. This impingement causing instantaneous liquefaction is possibly the

mechanism behind the liquid sample ejection. Also, a significant vortex ring near the target was observed in emission images. This occurs after the distortion of hemispherically occurring vapour plume with >100 ns laser pulse.

A physical model is proposed to calculate the recoil evaporation pressure acting on the surface of an evaporating material irradiated with high-intensity laser beam such as encountered in laser–material interaction. Laser attenuation in the laser-induced plasma plume, reflection at the surface material and the energy consumption for material heating and melt-vaporization are considered in this mode. The calculated plasma recoil pressures compare favourably with the experimental data reported by Richards and Walsh [8].

The physical and hydrodynamical condition for vaporization is dependent on the pressure p_{pl} in a plasma cloud and the saturated vapour pressure p_{sat} . If $p_{pl} > p_{sat}$, the vaporization process is slowed down and ultimately ceases to exist. Moreover, the shielding effect in the plasma leads to a change of the thermal parameters in the vicinity of the surface. This causes a change in the conditions of vaporization.

The Mach number M on the outer side of the Knudsen layer is the most important dimensionless parameter (in the subcritical region) which characterizes the magnitude of the reverse plasma flux and thereby relates to the vaporization processes in the flowing gas (plasma cloud). For saturated vapour pressure p_{sat} larger than the external pressure and at $M = 1$ (e.g., vaporization in vacuum) the processes occurring in the condensed and gaseous phase are independent of each other. In sonic regime ($M = 1$) and for a given surface temperature T_s , the material flux traversing across the boundary layer is maximized. The recoil pressure experienced by the surface is minimum at this instant.

In subsonic regime ($M < 1$), a stable vapour flow ensues when the plasma pressure gets balanced by external pressure. Under these circumstances gas dynamic variables will dictate the flow conditions. Such a scenario renders mathematical description of the process difficult. Further complications arise due to intervening phase transition among solid, liquid and gas. Assuming absence of recombination between solid and gaseous phases, a comprehensive physico-mathematical solution to the coupled differential equations governing interconnected phenomena like phase transition, gas dynamics and vaporization has not been attempted so far. However, the phase transition event has been dealt in isolation as investigated by Sy-Bor Wen *et al* [6] and Richards and Walsh [8].

The laser-plasma formation on the surface of Ti substrate is associated with thermal dynamics of intense surface vaporization and non-linear multiple thermal phase transitions. The present paper expedites solution of these coupled events in terms of non-stationary Eulerian variables. It is also revealed that the thermal instabilities pertaining to laser intensity and flux energy causes significant variation in Mach number. The physical properties of Ti have been detailed in table 1.

In the present model, a Ti target with thickness l is impacted with a laser radiation flux $I \geq 10^8$ W/cm² causing vaporization of the material surface. Both solid–liquid and liquid–vapour phase transitions accompany this event. While conduction–convection phenomenon is the dominant mode of energy transfer in the condensed phase, in gas phase such process involves absorption of laser flux and radiative flux emanating from the specimen surface causing dispensation of the excess energy.

Table 1. The phase transition properties of Ti.

Phase	Solid
Density	4.506 g cm ⁻³
Liquid density (near melting point)	4.11 g cm ⁻³
Melting point	1941 K (1668°C)
Boiling point	3560 K (3287°C)
Heat of fusion	14.15 kJ mol ⁻¹
Heat of vaporization	425 kJ mol ⁻¹
Heat capacity	(25°C) 25.060 J mol ⁻¹ K ⁻¹
Thermal conductivity	(300 K) 21.9 W m ⁻¹ K ⁻¹
Thermal expansion	(25°C) 8.6 μm m ⁻¹ K ⁻¹

It has been shown by spectroscopic measurements that laser beam focused on a material surface in vacuum gives a radiant temperature of the order of (8500 ± 1500) K as revealed from investigations by Semak *et al* [9]. More precisely, with a time-resolved spectrometric technique, the temperature rises to its peak value in 30 ns after the initiation of laser pulse and then falls with a thermal time constant of ~ 100 ns. The thermionic emission of electrons and ions was recorded. These are emission of two pulses separated in time by few tenths of ns. A simple qualitative theory is suggested which accounts for most of the experimental results. This involves charge separation from the plasma of vaporized material. This was found from the Langmuir probe measurements. An electron temperature of $\sim 10^5$ K was revealed from studies carried out by Richards and Walsh [8] and Semak *et al* [9].

The physico-mathematical description of the phase transition event associated with vaporization phenomena and subsequent oscillation in Knudsen layer involves conservation laws for mass, energy and momentum balance. The governing mathematical equations addressing boundary value heat conduction-convection problem as well as the conservation equation covering mass, energy and momentum balance have been described by Kumar *et al* [10]. In the present work the boundary value heat conduction-convection problem for condensed media is solved in a moving coordinate system to obtain expression for propagating vaporization front. This approach is similar to the one followed by Sy-Bor Wen *et al* [6] and Richards and Walsh [8]. The set of governing mathematical equations with necessary boundary conditions are outlined below for the sake of completeness:

$$\begin{cases} \rho(T)c(T) \left[\frac{\partial T}{\partial t} - v(t) \frac{\partial T}{\partial z} \right] = \frac{\partial}{\partial z} (\lambda(T) \frac{\partial T}{\partial z}) \\ z = -l, \quad \lambda(T) \frac{\partial T}{\partial z} = 0, \quad z = 0, \quad z = p \\ -\lambda(T) \frac{\partial T}{\partial z} = I_s + W_s - v_s \rho_s(T_s) L_v \\ z = x - \int_0^T v(T) dt, \quad I_s = (1 - R(T_s)) I \end{cases} \quad (1)$$

$$W_s = \int_0^\infty dv \int_{-1}^1 \mu I_v d\mu; \quad k_v = k_v(v, \rho, T). \quad (2)$$

In the above equations, t refers to the time coordinate whereas z is a spatial variable. Temperature-dependent heat capacity and thermal conductivity are described by $c(T)$ and $\lambda(T)$, respectively. $R(T_s)$ is the reflected laser radiation function at a given surface temperature T_s . v , ρ , p and T are the velocity, density, pressure, temperature and internal energy, respectively. I_s and W_s are the intensity and energy flux of the incident laser beam at the surface of the material, respectively. k_v is the absorption coefficient of laser radiation in the material at a given radiation frequency. ρ_s is the surface density of the material. The heat conduction equation, in two dimension, assumes the following form:

$$dQ = \left\{ \begin{array}{l} V_m dr \left[\frac{\partial T}{\partial z}(z + dz, r, t) - \frac{\partial T}{\partial z}(z, r, t) \right] \\ + V_m dz \left[\frac{\partial T}{\partial r}(z, r + dr, t) - \frac{\partial T}{\partial r}(z, r, t) \right] \lambda(T) dt \end{array} \right\}, \quad (3)$$

where V_m refers to volumetric heat conduction in the material.

If both the boundaries t and r are assumed to be at zero temperature, the solution will approach $u(r, t) = 0$ everywhere in the material. If both the boundaries are insulated, the solution will approach $u(r, t) = \text{constant}$. The heat is evenly distributed as $t \rightarrow \infty$. The conservation law is still obeyed. The finite difference approximation method is analysed to yield heat distribution in a given volumetric zone. These calculations can be carried out from the following governing equations:

$$\begin{cases} u(x, 0) = \delta(x); \quad u(x, t) = \frac{1}{\sqrt{4\pi t}} \exp^{-x^2/4t} \\ u(x, y, 0) = \delta(x)\delta(y); \quad u(x, y, t) = \left(\frac{1}{\sqrt{4\pi t}} \right)^2 \exp^{-x^2/4t} \exp^{-y^2/4t} \\ \text{erf}(x) = \frac{2}{\pi} \int_0^x \exp(-V_m)^2 dV_m; \\ u(x, t) = \frac{\sqrt{4t}}{\sqrt{4\pi t}} \int_{-x/\sqrt{4t}}^{\infty} \exp(-V_m)^2 V_m = \frac{1}{2} \left[1 + \text{erf} \left(\frac{x}{\sqrt{4t}} \right) \right]. \end{cases} \quad (4)$$

The integral in the range $-x$ to 0 is also $\text{erf}(x)$. The normalization by $2/\sqrt{\pi}$ gives $\text{erf}(\infty) = 1$. The error function from the integral heat conduction equation can be obtained by setting $V_m = (V_m - x)/\sqrt{4t}$. Then $s = 0$ yields $V_m = -x/\sqrt{4t}$ as lower limit and $dV_m = dV_m/\sqrt{4t}$. An integral from 0 to ∞ converts $-x/\sqrt{4t}$ to 0.

To find a generalized solution to the system of eqs (1)–(4), a numerical procedure based on iterative cycles was carried out with the following parameters: $l = 100 \mu\text{m}$, $l_1 = 20 \text{ cm}$ and $I \geq 10^8 \text{ W/cm}^2$. Values of the thermal constants $R(T_s)$, $\lambda(T)$, $c(T)$, $\rho_s(T_s)$ and saturated pressure $p_{\text{sat}}(T_s)$ for Ti were obtained from the literature data published by Semak *et al* [9]. The high-temperature values of $\lambda(T)$, $\rho(T_s)$ and $p_{\text{sat}}(T_s)$ were determined by non-linear interpolation between the last known value and its characteristic measure at the critical temperature $T_{\text{cr}} = 6000 \text{ K}$. A pulse of laser radiation has a Gaussian shape with a pulse duration of 5 ns. The results of the numerical modelling are presented in figure 1. The time dependence of the laser flux I_s and the radiative flux W_s absorbed by the surface are shown in figure 1a. The values of these fluxes determine surface temperature T_s . This, in turn, completely quantifies the saturation pressure $p_{\text{sat}}(T_s)$. The dependence of the saturation pressure p_{sat} and of the plasma pressure p_{pl} in the plasma (in the first computational interval from the surface) are shown in figure 1b. The ratio of values of these parameters determines the nature of variation of the Mach

number reported by Kumar *et al* [10]. From that result, it follows that the laser radiation flux arriving at the surface rapidly declines. This flux, initiated at breakdown instant, $t = 1.75$ ns, wanes out and gets completely shielded by the plasma cloud (figure 1a). The curves of $T_s(t)$ and $W_s(t)$ have two clearly pronounced peaks. The first peak is caused by the absorption of the laser flux I_s by the surface and is characterized by the values $T_s(\text{max}) = 0.64$ eV and $p_{\text{sat}} = 1998$ atmospheres. Here the pressure p_{sat} is greater than the pressure p_{pl} in the gaseous media. The vaporization regime with $M = 1$ corresponds to this time interval t . After the vaporization mass reaches the value $m \approx 2.3 \times 10^{-5}$ g cm $^{-2}$, the vapour becomes a medium which absorbs the laser radiation well. The radiation flux I_s at the surface decreases due to decrease in the value of T_s and p_{sat} ($T_s(\text{min}) = 0.26$ eV and $p_{\text{sat}}(\text{min}) = 10.3$ atm). At this instant, strong absorption of the laser radiation causes pressure and temperature of the plasma to shoot up. The pressure in the plasma becomes comparable to the saturation pressure and finally exceeds it (figure 1b). This leads to a very rapid reduction in Mach number ($M < 1$). The Mach number passes through a null point at $t = 1.5$ ns and turns negative ($M < 0$). The value $M = 0$ implies that there is no material flux traversing the phase separation boundary. This shows that there is no further vaporization. The negative value of Mach number reveals reversal in direction of gas discharge flux. The present model excludes condensation phenomena. A finite plasma flux density $\rho_{\text{pl}}u_1$ equaling $\rho_s V_s$ reaches the surface of the material. The increase in temperature of the plasma with simultaneous decreases in its density ρ_{pl} on account of gas dynamic expansion results in the appearance of powerful radiative flux W . The second peak of the curves $p_{\text{sat}}(t)$ is determined by the value of radiative flux W_s arriving at the surface ($W_s(\text{max}) = 6.8 \times 10^7$ W/cm 2 at $t = 1.75$ ns). Under the action of flux W_s , the surface temperature increases with concomitant increase in value of saturation pressure p_{sat} till it overcomes plasma pressure p_{pl} . The negative value of M is reduced (the maximum of $M = -0.3$ occurs at $t = 2$ ns) and then becomes positive again initiating a new period of vaporization (from $t = 2.5$ ns to $t = 3.5$ ns).

The secondary vaporization results in attenuation of the flux W_s . After a lapse of $t = 1.75$, the plasma pressure exceeds saturation pressure ($p_{\text{pl}} > p_{\text{sat}}$). At this instant Mach number has a subzero value ($M < 0$). This scenario prevails till the termination of the laser pulse at 3.5 ns. The physical condition for occurrence of plasma near the surface of the condensed media are qualitatively different for vaporization phenomena in subsonic ($M < 1$) and near sonic ($M = 1$) regimes. Under supersonic conditions ($M > 0$) and under the influence of plasma, the vaporization occurs in two short time-step intervals. During the remaining instants, no vaporization is observed owing to the prevalence of high plasma pressure.

The solution of the partial differential equations (1) and (3) addressing to the heat conduction problem yields temporal evolution of temperature profile in the material shown in figure 2. Maximum value of temperature attained by a material depends upon incident laser power density. A peak temperature of 646°C is reached with a laser power density 1 J/cm 2 . However, this value swiftly declines to 105°C over a period of ~ 1 ns due to rapid thermal conduction. The recorded peak temperature at 3 J/cm 2 is 1200°C which declines to 550°C after ~ 1 ns. The peak temperature recorded at 3 J/cm 2 is nearly twice the value obtained for 1 J/cm 2 of

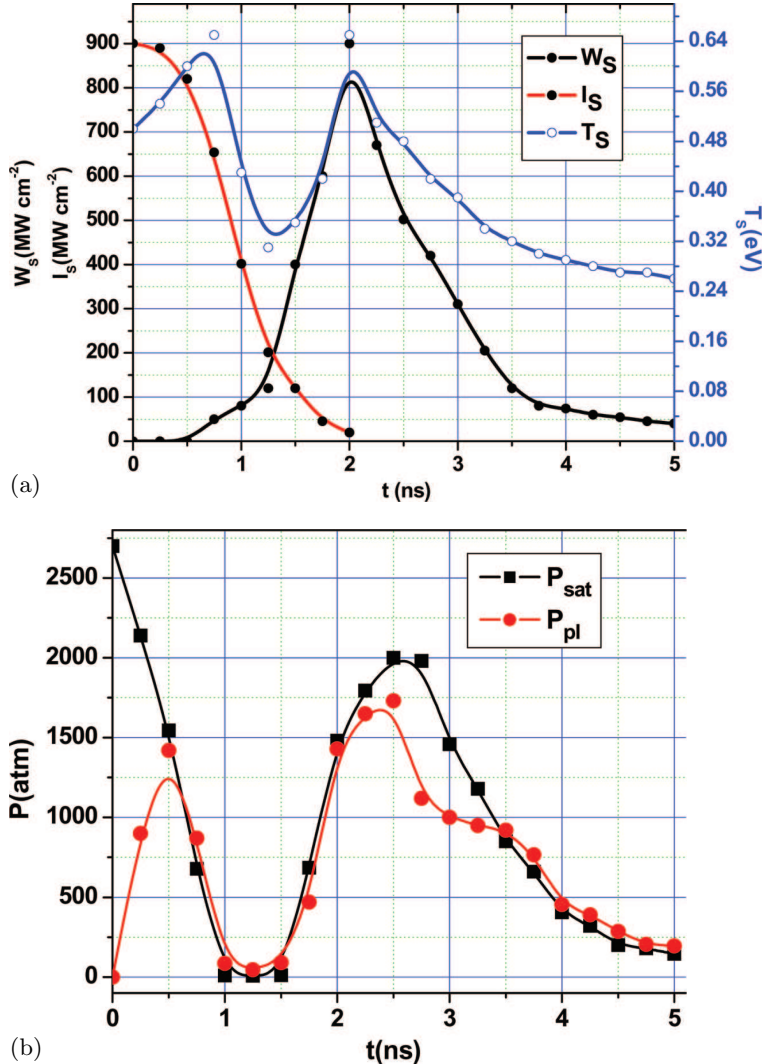


Figure 1. The results of the numerical modelling. **(a)** The time dependences of the laser flux I_s and the radiative flux W_s that are absorbed by the surface. **(b)** The time dependencies of the saturation pressure p_{sat} and of the plasma pressure p_{pl} in the plasma (in the first computational interval from the surface).

surface laser power density. At 5 J/cm 2 , the value of temperature shoots to 1834°C and declines to 835°C after a lapse of \sim 1.2 ns. In accordance with the computation, it can be stated that the range of temperature distribution in material is a function of incident laser power density. However, the subsequent rate of decline does not depend on incident power density. Thermal conductivity of the condensed

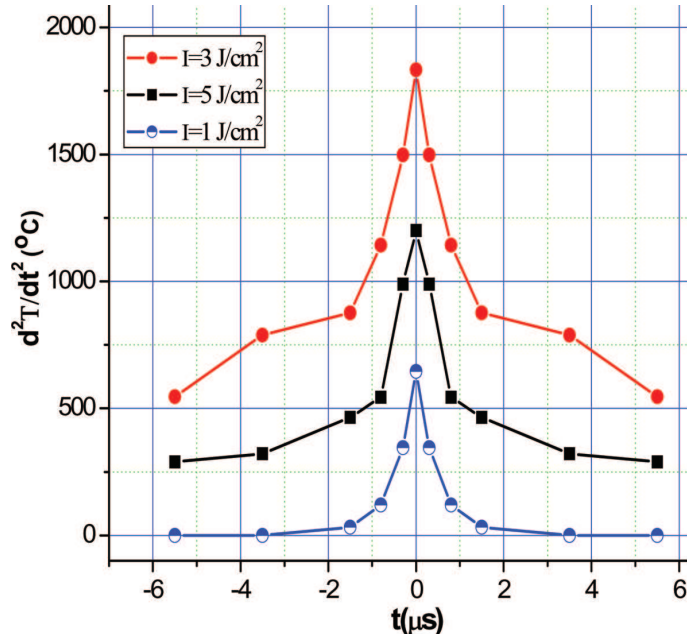


Figure 2. Thermal conduction-based temperature profile in material as a function of incident laser power density.

medium, being the sole deciding factor, brings out almost equal decay periods. These numerically computed results are in conformity with the experimental data published by Samokhin [18]. Slightly lower thermal conductivity of the material at high temperature accounts for a slightly higher decay period of ~ 1.2 ns due to lower rate of power dissipation.

3. Heat conduction across thermal boundary layer

In many laser applications it is the conversion of photon energy to heat which drives the process forward. Heat transfer theory accurately describes the effects produced. Other aspects of thermodynamics need not be considered explicitly for the computations. The highly non-equilibrium nature of laser material processing operations can usually be ignored once the heat transfer problem is correctly defined. However, 'equilibrium' is a concept that is based on thermodynamic phenomena. Hence it is useful to examine this concept in the context of traditional laser–material interaction. Some of the assumptions associated with the adoption of equilibrium solutions are discussed by Chung and Das [11]. The role of surface reconstruction and entropy in achieving an equilibrium state is evaluated. Surface tension effects and work done during laser–material interaction are also investigated. It is concluded that the path to achieve steady-state process in laser–material interaction requires quantitative application of geometrical as well as thermodynamic parameters.

The calculations based on the hydrodynamic physical model of laser–material interaction includes the effect of evaporation recoil pressure on melt flow and the consequent convective heat transfer. The computations follow an experimentally verified physical model of melt hydrodynamics and the model of laser-induced evaporation reported by Zhang and Faghri [12]. The simulations indicate that convective heat transfer which is induced by recoil pressure has a significant amount of absorbed intensity ranging between 0.5 and 10 MW cm⁻². This range corresponds to laser welding, cutting and drilling due to melt ejection (hydrodynamic drilling). The simulations also show that the motion of the melt from the centre of the interaction zone towards the periphery results in a secondary maximum in the temperature distribution. This, in turn, can lead to instability of the melt flow and temperature field fluctuations. The model also predicts that the cooling rate in and around the fusion zone is strongly influenced by the recoil pressure-induced melt flow. At the centre of the beam interaction zone the cooling rate is higher (~10 times). At the periphery it is lower than the rates predicted from the heat conduction model.

There are two widely used methods in the fixed grid solution for addressing these phase change problems. These are enthalpy method and temperature-based equivalent heat capacity method described by Ki *et al* [13]. Enthalpy methods are flexible and can deal with phase change problems occurring both at a single temperature and over a wide temperature range. However, these methods have shortcomings. Although the predicted temperature distribution and melting fronts are easily obtained, the predicted time history of the temperature at a typical grid point may depict some oscillations. The temperature-based fixed grid methods have no such time history problems and are more convenient to deal with conjugate problems involving an adjacent wall. However, non-linearity of the governing equations at the phase change temperature needs to be addressed. This range is rather small. On the other hand, front tracking schemes attempt to explicitly track the interface using the Stefan condition. While one approach is to fix the spatial step but allow the time step to float in such a way that the front always passes through a node, the other approach is to fix the time step and allow the spatial step to float using two distinct time-varying spatial steps for the two phase fluid flow. Although such approaches work fairly well for a simple Stefan problem, difficulties arise when the entire domain is at the same initial temperature. This is far below the melting temperature. An *a priori* knowledge of initial melt interface location is required. Here we develop a front tracking scheme with fixed grid and fixed time step based on a finite volume method with Laplace differential transformation. An explicit discretization scheme (first order in time domain, second order in space domain) satisfying stability criteria of the Laplace differential transformation, is developed.

The dependence of saturation temperature on the back pressure of the material is taken into account using the Clausius–Clapeyron equation. The conduction of heat loss to the solid is also included in the model which is solved using an integral approximate method described by Lugomer [14]. The results show that the fraction of the heat lost through conduction to the solid is very small and its effect on the vaporization process is not significant. On the other hand, the conduction heat loss significantly reduces the thickness of the liquid layer which becomes a recast layer after the vaporization event.

When liquid-vapour interface temperature reaches the boiling point, evaporation begins to occur. It is shown that there exist a very thin layer of several mean free paths known as kinetic Knudsen layer just outside the liquid-vapour interface. Across this layer the continuum hypothesis fails and steep changes in temperature, pressure and density occurs. It has been reported by Zabusky *et al* [15] that homogeneous boiling of the skin layer of material starts to occur directly beneath the liquid-vapour interface when the interface temperature reaches around 80% of the critical point. This accompanies a significant drop in the surface tension and huge amount of melt liquid superheat.

The purpose of forward heat conduction problem is to map out the spatial temperature distribution for a given system configuration. For a two-dimensional heat conducting media with uniform thermal conductivity, the higher-order Laplace partial differential equation in cylindrical coordinates can be written as follows:

$$\begin{cases} \nabla^2 T \left(\frac{\partial T}{\partial r} + \frac{\partial T}{\partial z} \right) = 0; & \left(\frac{\partial T}{\partial r} + \frac{\partial T}{\partial z} \right) \in \Gamma_D \\ \text{or, } \nabla^2 T(r, z) = 0; & (r, z) \in \Gamma_D \end{cases} . \quad (5)$$

Equation (5) can be considered in two-dimensional heat conduction processes in a finite cylinder. Then the governing equation assumes the following form:

$$\frac{\partial^2 T}{\partial r^2} + \frac{1}{r} \frac{\partial T}{\partial r} + \frac{\partial^2 T}{\partial z^2} = -\frac{g(r, z)}{k} . \quad (6)$$

A physical interpretation of this approach, called the method of descent, distributes 3D point sources to form a ring-shaped source appropriate for axisymmetric 2D heating. In a forward problem, one of the following three linear boundary conditions can be imposed on any position or on the entire system. These boundary conditions are:

$$\begin{cases} \text{Dirichlet: } T(r, z) = T, & (r, z) \in \Gamma_D \\ \text{Neuman: } -\lambda(T) \nabla T(r, z) \times \hat{n}(r, z) = q(r, z), & (r, z) \in \Gamma_N \\ \text{Robin: } -\lambda(T) \nabla T(r, z) \times \hat{n}(r, z) = h[T(r, z) - T_\infty], & (r, z) \in \Gamma_R \end{cases} . \quad (7)$$

$T(r, z)$ denotes the temperature evaluated at the surface of the material. $\nabla T(r, z)$ describes the corresponding temperature gradient. The Dirichlet formalism yields temperature distribution in radial and axial directions $T(r, z)$ at the material surface. The Neuman condition prescribes the surface heat flux distribution in the radial and axial directions $q(r, z)$ of the intercepting surface. The outward drawn normal is $\hat{n}(r, z)$. The Robin condition prescribes convective-conduction at the surface, which convects heat with a convective film heat transfer coefficient h to the surroundings at an ambient temperature T_∞ . Results, from the calculation through eqs (3) and (6) with given boundary conditions (7), are as following. At a Mach number value $M > 0.42$ and time at $t = 0.5$ ns, the temperature in axial and radial directions, i.e., both $T(z)$ and $T(r)$ get maximized. Absorption of laser radiation is completed in this regime, i.e. $0.42 < M < 0.42$. After attainment of peak temperature, a decline is observed in both radial and axial directions. This

decline is attributed to the onset of diffusion and heat convection in material as well as absorption of laser radiation in plasma plume. The computed values of peak temperature as reported by Kumar *et al* [10] works out to $T(r) = 5300^\circ\text{C}$ and $T(z) = 5980^\circ\text{C}$. The Gaussian profile of beam is concentrated more in axial direction which causes high laser energy to be dissipated axially.

During the course of laser–material interaction, a series of sequential phenomena ensues. In accordance with the reported experimental data presented by Mazhukin *et al* [16] and Mirzoev [17] and experiments performed in 5–6 J/cm² energy density, the following inferences can be drawn:

1. In the case of laser interaction time interval 0–10 ns, the beam strikes the surface and melts it within ~ 3 ns to a depth of $h \leq 3 \mu\text{m}$ in the centre and $h \sim 1 \mu\text{m}$ at the periphery of a Gaussian spot. The radius of the melted zone ranges from ~ 1 to 1.1 mm while the radius of a blast wave affected zone ranges from 0.60 to 0.80 mm. This point has an observable zone in which the shock accelerated melted material gets translated radially. The radius of a heat affected zone is 1.8 mm. The spot area increases because of plasma expansion and the close contact that exist with the target surface. The initial impact of the laser beam generates surface waves in metal which propagate outward with a velocity of $\geq 10^3 \text{ m/s}$.
2. The beam vaporizes the central region into a plume which rises ~ 2 mm above the surface. This is estimated on the basis of the size of a luminous plasma cloud.
3. The beam ionizes the plume to a maximum temperature $\geq 10^4 \text{ K}$. This estimate agrees with the literature reports. This sudden temperature surge causes explosion and formation of a blast wave.

In the case of time interval 10–30 ns, the blast wave is formed after ~ 10 ns, i.e. with a delay of $\sim 1/3\tau - 1/2\tau$ with respect to the onset of the laser pulse. The supersonic blast wave moves up and over the surface it registers a velocity of $\sim 10^6 \text{ cm/s}$. This reaches a peak pressure of ~ 10 –20 kbar. Once the blast wave has been initiated, the pulse delivered to the surface is primarily due to the air shock produced above the surface of the material. Therefore, the theoretical analysis of the above processes is formulated based on blast wave-induced shock phenomena.

Normalized time interval over which the initial blast wave vertically propagates amounts to the half-width of the domain. This wave finally arrives at the bottom of the target. At $t = 0.5$, blast wave propagating upward passes through the upper non-reflective boundary while its left and right components are reflected away from the vertical boundaries. This reflected wave does not play any significant role. At $t = 1.25$, the downward moving blast wave gets reflected from the lower boundary. This reflected upwardly mobile shock wave overtakes and interacts with the vertically moving contact zone. The wavelengths, especially the longer ones, were compared with initial estimates. This wavelength is possibly associated with the transition length (thickness) of the contact zone. This wavy structure persists as it moves upward and could be related to some of the structures observed experimentally by Mirzoev [17].

3.1 Condensed phase

Process of energy transfer across the condensed phase domain boundary is governed by heat conduction equation described by Samokhin [18]:

$$\begin{cases} \frac{\partial H}{\partial t} + V_{re} \frac{\partial H}{\partial z} = -\operatorname{div} \vec{\mathbf{W}} \\ H_c = \rho \lambda(T) T \\ \vec{\mathbf{W}} = -\operatorname{grad} T \end{cases} . \quad (8)$$

Here c is an index that denotes the condensed phase. T , H and $\vec{\mathbf{W}}$ are the temperature, volumetric enthalpy and heat flux, respectively. V_{re} is the surface recession velocity (interface velocity). ρ and $\lambda(T)$ are the density and thermal conductivity, respectively. The external boundaries of the condensed domain are heat-insulated with initial target temperature being $T_0 = 300$ K.

3.2 Gaseous phase and plasma

When the laser intensity is large enough, i.e. nearing $\sim 10^9$ W/cm², optical thickness of the evaporated substance is sufficient to initiate an intensive absorption coupled to ionization. The resulting vapour plasma is partially or completely opaque for laser radiation. The energy balance is due to the work done by plasma pressure and energy linked to thermal radiation as reported by Samokhin [18]. In the vapour plasma domain, the system of equations for radiation gas dynamics (RGD) is written as reported by Samarkin and Popov [19]:

$$\frac{\partial \rho}{\partial t} + \operatorname{div}(\rho \vec{\mathbf{V}}) = 0 \quad (9)$$

$$\rho \frac{\partial \vec{\mathbf{V}}}{\partial t} + \rho(\vec{\mathbf{V}} \times \nabla) \vec{\mathbf{V}} = -\operatorname{grad} p \quad (10)$$

$$\frac{\partial(\rho e)}{\partial t} + \operatorname{div}(\rho e \vec{\mathbf{V}}) = -p \operatorname{div} \vec{\mathbf{V}} - \operatorname{div} \vec{\mathbf{q}} + \frac{\partial \mathbf{G}}{\partial z} \quad (11)$$

$$\begin{cases} \operatorname{div} \vec{\mathbf{q}}_v + k_v U_v = k_v U_{bv}; \\ \vec{\mathbf{q}}_v = -\frac{1}{3k_v} \operatorname{grad} U_v; \\ U_{bv} = \frac{8\pi h v^3}{c^3 [\exp(\hbar v/kt) - 1]}; \\ \vec{\mathbf{q}} = \int_v \vec{\mathbf{q}}_v dv \end{cases} \quad (12)$$

$$p = p(\rho, T), \quad e = e(\rho, T), \quad k_v = k_v(\rho, T, v) \quad (13)$$

$\vec{\mathbf{V}} = (u, v)$ is the gas-dynamic velocity. ρ , p and e are the density, pressure and volumetric internal energy, respectively. k is the Boltzmann constant, \hbar is the Planck

constant, $\vec{q} = (q_r, q_z)$ is the vectoral radiative heat flux, κ_v is the absorption coefficient of plasma radiation, U_v , U_{bv} are the volumetric density of radiation and black body radiation. v denotes frequency-dependent quantities that describe radiation transfer. The system of equations (9)–(13) is supplemented by the boundary conditions which are based on the Hartree–Fock–Slater model. Laser radiation transfer equation along the z -axis accounts for incident G^- and reflected G^+ components. The self-consistent model is applied which include the heat transfer equation in condensed medium, the equations of radiation gas dynamics in evaporated substance and the Knudsen layer model at the media boundary. It is found that the phase transition at the target surface is controlled by two factors: the surface temperature that depends on the transmitted radiation intensity and the plasma pressure governed by the expansion regime. The process comes through three characteristic stages: the sonic evaporation at the beginning, the condensation during the period of plasma formation, initial expansion and the re-start of evaporation in the subsonic regime after the partial brightening of the plasma. During the subsonic evaporation stage, the vapour flow and the mass removal rates are much higher near the beam boundaries than in the centre due to prevalence of smaller plasma counter-pressure. The vapour plasma pattern is characterized by the dense hot zone near the surface where the absorption of laser energy occurs. The density outside this absorption zone is reduced due to three-dimensional expansions.

4. Conclusion

It is observed that in the laser-induced vaporization process, Mach number M on the outer side of the Knudsen layer is the most important transport parameter in the subcritical region which characterizes the magnitude of the reverse plasma flux and thereby relates to the vaporization processes amidst plasma cloud. For saturated vapour pressure p_{sat} exceeding external pressure and at $M = 1$, the material flux across the boundary layer is maximum and vapour recoil pressure experienced by the surface is minimum. These correspond to a particular surface temperature T_s . From these results it follows that the flux of laser radiation reaching the surface decreases rapidly. This decline has its inception from the moment of breakdown at $t = 1.75$ ns and ends with complete shielding of flux by the plasma. In this case, no more laser energy is left for absorption by the material as the entire energy gets absorbed by the plasma cloud propagating outward from the material surface. Consequently, surface temperature of the material is drastically diminished. When Mach number $M = 0.42$, the temperature and the rate of the evaporation achieve maximum value due to collapse of plasma cloud at $t = 0.5$ ns. Peak values of the temperature and evaporation rate are no more definable due to secondary growth of plasma cloud which propagates outward from the material surface. So, more laser energy will be absorbed in the plasma leading to intense condensation at the material surface. It is explained that under the influence of the plasma, vaporization occurs in two short time intervals ($t = 1.5$ ns) where $M > 0$. Despite the high surface temperature, no vaporization occurs during the remaining time because of prevalence of high pressure in plasma which nearly equals to saturation

pressure. When $M = 0.4$ at $t = 0.5$ ns, the plasma pressure and the saturation pressure are nearly equal. At this instant the surface temperature achieves maximum value ($T_s(\max) = 0.64$ eV) due to maximum laser energy absorption in condensed phase.

References

- [1] V V Semak and A Matsunawa, *J. Phys.* **D30**, 2541 (1997)
- [2] Radovan Gospavic and Milesa Serkovic, *Mathematics and Computers in Simulation* **65**, 211 (2004)
- [3] B N Chichkov, C Momma, S Nolte, F von Alvensleben and A Tunnermann, *Applied Physics A: Materials Science & Processing* **63(2)**, 109 (1996)
- [4] Jun-Ho Cho, Suck-Joo Na, *J. Phys.* **D40**, 7638 (2007)
- [5] M D Shirk and P A Molian, *J. Laser Applications* **10(1)**, 18 (1998)
- [6] Sy-Bor Wen, Xianglei Mao, Ralph Grief and Richard E Russo, *J. Appl. Phys.* **101**, 023115 (2007)
- [7] Xi Chen and Hai-Xing Wang, *J. Phys.* **D34**, 2637 (2001)
- [8] F A Richards and D Walsh, *Brit. J. Appl. Phys. (J. Phys. D)*, Ser. 2, **2**, 663 (1969)
- [9] V V Semak, B Damkroger and S Kempka, *J. Phys.* **D32**, 1819 (1999)
- [10] N Kumar, S Dash, A K Tyagi and B Raj, *Science and Technology of Welding and Joining* **12**, 540 (2007)
- [11] Haseung Chung and Suman Das, *Int. J. Heat and Mass Transfer* **47(19)**, 4153 (2004)
- [12] Y Zhang and A Faghri, *Int. J. Heat and Mass Transfer* **42(10)**, 1775 (1999)
- [13] H Ki, P S Mohanty and J Mazumder, *J. Phys.* **D34**, 364 (2001)
- [14] Stjepan Lugomer, *Phys. Lett.* **A361**, 87 (2007)
- [15] N J Zabusky, S Lugomer and S Zhang, *Fluid Dynamics Research* **36**, 291 (2005)
- [16] V I Mazhukin, V V Nosssov and I Smurov, *Thin Solid Films* **453–454**, 353 (2004)
- [17] F Kh Mirzoev, *Kvantovaya Elektronika* **24(2)**, 138 (1994)
- [18] A A Samokhin, *Kvantovaya Elektronika* **10(10)**, 2022 (1983)
- [19] A A Samarkin and Yu P Popov, *Nauka (Moscow)* **12**, 22 (1984)